Raman amplification of optical pulses in silicon waveguides: effects of finite gain bandwidth, pulse width, and chirp

Samudra Roy,[1] Shyamal K. Bhadra,[1,*] and Govind P. Agrawal[2]

[1]*Central Glass and Ceramic Research Institute (CGCRI) under Council of Scientific and Industrial Research (CSIR), 196 Raja S. C. Mullick Road, Kolkata-700032, India*

[2]*Institute of Optics, University of Rochester, Rochester, New York 14627, USA*

[*]*Corresponding author: skbhadra@cgcri.res.in*

Received September 11, 2008; revised October 15, 2008; accepted October 16, 2008; posted October 21, 2008 (Doc. ID 101393); published December 10, 2008

We present a theoretical model capable of describing the evolution of pulse parameters when stimulated Raman scattering under continuous-wave pumping is employed for amplifying them inside a silicon waveguide. In our approach, pulse evolution is described analytically by a set of coupled equations derived using a variational formalism. Optical losses resulting from linear absorption or scattering, two-photon absorption, and free-carrier absorption are included by introducing the Rayleigh dissipation function. The influence of gain dispersion originated from a relatively narrow Raman-gain bandwidth is also considered. The role of initial pulse width and chirp is studied extensively because of its practical applications. To ensure the validity of the variational technique, all analytical results are compared with the numerical data obtained with the split-step Fourier algorithm.

OCIS codes: 190.3270, 190.5650.

1. INTRODUCTION

The topic of silicon photonics has attracted a great deal of attention in recent years owing to its promising applications in the fields of optical telecommunications and optoelectronic integration [1]. Silicon waveguides, fabricated with silicon-on-insulator (SOI) technology, play the role of the so-called photonic wires in the spectral region beyond 1100 nm because they can confine an optical field tightly, within a submicron region, without introducing linear absorptive losses. Moreover, for such silicon waveguides, the nonlinear Kerr coefficient is more than 100 times larger and the Raman gain coefficient is nearly 10,000 times larger than those of the silica fibers that are generally used for telecommunication applications. Such high values of the Raman gain and the Kerr coefficients result in efficient nonlinear interaction of light at relatively low power levels in a waveguide only a few millimeters long. Recent results indeed show that the well-known nonlinear phenomena such as self-phase modulation (SPM) [2], cross-phase modulation (XPM) [3], stimulated Raman scattering (SRS) [4–16], four-wave mixing [17], and supercontinuum generation [18] can easily occur within SOI waveguides, and they can be exploited for a variety of applications.

In this work, we focus on the nonlinear phenomenon of Raman amplification of optical pulses within a SOI waveguide. It is well known [5–10] that the efficiency of the Raman process can be degraded considerably by the nonlinear process of two-photon absorption (TPA), mainly because it leads to significant accumulation of free carriers within the waveguide at high pump powers. Because of its nonlinear nature, TPA increases rapidly with increasing pump intensity, resulting in the generation of many free carriers, whose population decays slowly because of a relatively long carrier lifetime associated with silicon [8]. This population of free electrons and holes not only introduces additional optical losses through free-carrier absorption (FCA) [7,11] but also changes the refractive index of the optical mode [19,20]. As a solution to the FCA problem, a p-i-n structure along the rib waveguide is sometimes employed [13–16]. When a reverse bias is applied to the p-i-n diode, the TPA-generated electron-hole pairs are swept toward the p and n regions by the resulting strong dc electric field. The drift time of carriers then becomes the effective carrier lifetime, if it is the shorter one of the two times. The implantation of helium ions is also employed with success for reducing the lifetime of carriers in SOI waveguides [21,22]. In another technique, picosecond pulses with a low duty cycle ($<$100 MHz) are employed for Raman pumping. A relatively low duty cycle allows the free carriers generated by one pulse to recombine before the next pulse arrives. However, pulsed pumping is often impractical in practice because it suffers from walk-off effects, requires a mode-locked laser capable of generating short optical pulses, and also leads to distortion of signal pulses being amplified. Pulse parameters, such as the width and the frequency chirp associated with a signal pulse, may change even under continuous-wave (CW) pumping. However, not much attention has been paid so far to such effects.

In the present work we focus on the case of CW pumping [23] and study Raman amplification inside a SOI waveguide of an optical signal in the form of picosecond pulses. Our objective is to investigate how the nonlinear

process such as SPM, XPM, TPA, and the free-carrier population affect the signal pulse during its amplification. However, a relatively narrow bandwidth of the Raman gain spectrum ($\Delta\nu_R \approx 105$ GHz) in silicon indicates that pulses shorter than 50 ps would suffer from gain dispersion, an effect that has not been investigated so far. In this work we focus on the effects of a finite Raman gain bandwidth on the amplified pulse. For this purpose, we develop a semi-analytical model based on the variational formalism. Normally, the variational technique cannot be used in the presence of the Raman gain and the linear and nonlinear losses. However, we employ the Rayleigh dissipation function (RDF) [24,25] whose use allows us to extend the variational formalism to the case of Raman amplification while including the influence of TPA, FCA, and gain dispersion. The RDF is a well-known function in classical mechanics, and it is frequently used to solve dissipative frictional problems. The only major disadvantage of a variational technique is that its use requires one to assume a specific pulse shape that does not change during propagation. However, pulse parameters such as the amplitude, width, phase, and chirp are allowed to evolve during Raman amplification. In this work, we choose a Gaussian shape for signal pulses for convenience but note that the analysis can be extended for other pulse shapes.

2. THEORETICAL MODEL

We assume that a CW pump beam and a train of short signal pulses are launched into a SOI waveguide such that the frequency difference between the pump and the signal nearly equals the well-known Raman shift of 15.6 THz for silicon [4–6]. Each signal pulse propagating through the SOI waveguide is affected by the nonlinear processes of SPM, XPM, SRS, and TPA. The frequency dependence of the Lorentzian Raman gain profile is approximated as $g(\omega) \approx g_R\{1 - T_2^2(\omega - \omega_0)^2\}$, where g_R is the peak Raman gain and $T_2 = (\pi\Delta\nu_R)^{-1}$. The signal propagation through the SOI waveguide is governed by the following extended nonlinear Schrödinger equation [3,4] involving the free-carrier density N_c [19,20]:

$$\frac{\partial E_s}{\partial z} + \frac{i\beta_2}{2}\frac{\partial^2 E_s}{\partial t^2} = ik_s n_2(1+ir)(|E_s|^2 + 2|E_p|^2)E_s - \frac{\sigma_s}{2}(1+i\mu)N_c E_s - \frac{\alpha_s}{2}E_s + \frac{g_R}{2}\left[1 + T_2^2\frac{\partial^2}{\partial t^2}\right] \times |E_p|^2 E_s, \tag{1}$$

where E_p is the pump field, $k_s = 2\pi/\lambda_s$ is the wave number at the signal wavelength λ_s, n_2 is the nonlinear Kerr coefficient, $r = \beta_{\mathrm{TPA}}/2k_s n_2$ governs the relative importance of TPA, β_{TPA} is the TPA coefficient, σ_s governs the magnitude of FCA, and the parameter μ (with a value of about 7.5 for silicon) incorporates the refractive-index changes produced by free carriers. Further, N_c is the free-carrier density, β_{2s} is the group-velocity dispersion parameter, and α_s accounts for linear losses of the signal. The finite Raman gain is included through the last term with $T_2 \approx 3$ ps for silicon.

The pump evolution is governed by a similar equation. However, the dispersion term can be neglected for a CW pump. Further, if the pump is much more intense than the signal, the latter cannot affect it much through XPM. Pump depletion through SRS can also be ignored for the same reason. With these simplifications, the pump equation takes the following simple form:

$$\frac{dE_p}{dz} = ik_p n_2(1+ir)|E_p|^2 E_p - \frac{\sigma_p}{2}(1+i\mu)N_c E_p - \frac{\alpha_p}{2}E_p. \tag{2}$$

Here, k_p equals $2\pi/\lambda_p$ at the pump wavelength λ_p, and the subscripts s and p stand for the signal and pump, respectively. Notice that the pump field enters in Eq. (1) only through its power, $P_p = |E_p|^2 a_{\mathrm{eff}}$, where a_{eff} is the effective mode area within the SOI waveguide. It is thus useful to write an equation for P_p. The result is

$$\frac{dP_p}{dz} = 2a_{\mathrm{eff}}\mathrm{Re}\left[E_p^*\frac{dE_p}{dz}\right] = -\left[\frac{2k_p n_2 r}{a_{\mathrm{eff}}}P_p^2 + \sigma_p N_c P_p + \alpha_p P_p\right]. \tag{3}$$

Physically, the first term in the right-hand side of Eq. (3) is due to TPA, the second term accounts for FCA, and the third term represents the linear loss.

The theoretical model will be complete once we supplement it with a rate equation satisfied by the free-carrier density N_c. Free carriers are generated inside the SOI waveguide dominantly by the CW pump, if we assume that the peak signal power remains much smaller than the pump power over the entire waveguide length. Including various sources of nonradiative recombination of TPA-generated electron-hole pairs, this rate equation is given by [18–20,26–31]

$$\frac{dN_c}{dt} = \frac{\beta_{\mathrm{TPA}}}{2h\nu_p a_{\mathrm{eff}}^2}P_p^2 - \frac{N_c}{\tau_c}, \tag{4}$$

where $h\nu_p$ is the pump-photon energy and τ_c is the carrier lifetime (or recombination time), which may depend on the waveguide geometry because of surface recombination [26]. In the case of a CW pump, N_c does not vary with time and we can use the following steady-state solution [32]:

$$N_c(z) = \frac{\beta_{\mathrm{TPA}}\tau_c P_p^2(z)}{2h\nu_p a_{\mathrm{eff}}^2}. \tag{5}$$

Note that, even though under CW pumping the free-carrier density is constant over time, it changes with the propagation distance z because the pump power varies with z according to Eq. (3). Its average value $\bar{N}_c$ can be obtained by averaging the pump power over the waveguide length:

$$\bar{N}_c = \frac{\beta_{\mathrm{TPA}}\tau_c \bar{P}_p^2}{2h\nu_p a_{\mathrm{eff}}^2}, \quad \bar{P}_p = \frac{1}{L}\int_0^L P_p(z)dz. \tag{6}$$

3. DETAILS OF THE VARIATIONAL TECHNIQUE

Owing to its complexity, the signal equation (1) should be solved numerically. However, a numerical solution does not provide much physical insight, and it is difficult to explore the vast parameter space. The variational formalism allows us to convert Eq. (1) into a set of ordinary differential equations satisfied by the parameters associated with the signal pulse. As mentioned earlier, we make use of the RDF to include the gain and loss terms appearing in Eq. (1). The corresponding Lagrangian function and the RDF are found to be

$$L = \frac{1}{2}(E_s E_{sz}^* - E_s^* E_{sz}) + \frac{i\beta_{2s}}{2}|E_{st}|^2 + \frac{ik_s n_2}{2}|E_s|^4 + \frac{2ik_s n_2 P_p}{a_{\text{eff}}}|E_s|^2 - \frac{i\sigma_s \mu}{2}N_c|E_s|^2, \tag{7a}$$

$$R = \beta_{\text{TPA}}\left[\frac{1}{2}|E_s|^2 + \frac{P_p}{a_{\text{eff}}}\right](E_s E_{sz}^* - E_s^* E_{sz}) + \left[\frac{\sigma_s}{2}N_c + \frac{\alpha_s}{2} - \frac{g_R}{2a_{\text{eff}}}P_p\right](E_s E_{sz}^* - E_s^* E_{sz}) - \frac{g_R P_p T_2^2}{2a_{\text{eff}}}(E_{stt}E_{sz}^* - E_{stt}^* E_{sz}), \tag{7b}$$

where $E_{sz} = \partial E_s/\partial z$, $E_{st} = \partial E_s/\partial t$, $E_{stt} = \partial^2 E_s/\partial t^2$, and we have made use of the relation $P_p = |E_p|^2 a_{\text{eff}}$.

The next step is to assume a specific shape for the signal pulse. Although the method can be used with other pulse shapes as well, we choose the Gaussian shape and assume that the signal field has the following form:

$$E_s(z,t) = A_s \exp\left[-(1-ic_s)\frac{t^2}{2T_s^2} + i\varphi_s\right], \tag{8}$$

where A_s, T_s, φ_s, and c_s are, respectively, the amplitude, width, phase, and frequency chirp associated with the signal pulse at a distance z. Note that all four pulse parameters are allowed to vary with z. We now insert Eq. (8) into Eqs. (7a) and (7b) and calculate the reduced Lagrangian and the RDF using the relations [33]

$$L_g = \int_{-\infty}^{\infty} L\,dt, \quad R_g = \int_{-\infty}^{\infty} R\,dt. \tag{9}$$

The explicit expressions of L_g and R_g are found to be

$$L_g = -iA_s^2 T_s\sqrt{\pi}\left[\frac{\partial\varphi_s}{\partial z} + \frac{1}{4}\frac{\partial c_s}{\partial z} - \frac{c_s}{2T_s}\frac{\partial T_s}{\partial z}\right] + \frac{i\beta_{2s}\sqrt{\pi}}{4T_s}A_s^2[1+c_s^2] + \frac{ik_s n_2}{2\sqrt{2}}\sqrt{\pi}A_s^4 T_s + \frac{2ik_s n_2}{a_{\text{eff}}}P_p A_s^2 T_s\sqrt{\pi} - \frac{i\sigma\mu}{2}\left\{\frac{\beta_{\text{TPA}}\tau_c P_p^2}{2h\nu_p a_{\text{eff}}^2}\right\}A_s^2 T_s\sqrt{\pi}, \tag{10}$$

$$R_g = -i\left(\frac{\beta_{\text{TPA}}}{\sqrt{2}}\right)\sqrt{\pi}A_s^4 T_s\left[\frac{\partial\varphi_s}{\partial z} + \frac{1}{8}\frac{\partial c_s}{\partial z} - \frac{c_s}{4T_s}\frac{\partial T_s}{\partial z}\right] - 2iA_s^2 T_s\sqrt{\pi}\left[\frac{\partial\varphi_s}{\partial z} + \frac{1}{4}\frac{\partial c_s}{\partial z} - \frac{c_s}{2T_s}\frac{\partial T_s}{\partial z}\right]\left[\frac{\beta_{\text{TPA}}}{a_{\text{eff}}}P_p + \frac{\sigma_s}{2}\left\{\frac{\beta_{\text{TPA}}\tau_c P_p^2}{2h\nu_p a_{\text{eff}}^2}\right\} + \frac{\alpha_s}{2} - \frac{g_R}{2a_{\text{eff}}}P_p\right] - 2i\frac{g_R P_p T_2^2 A_s^2\sqrt{\pi}}{2a_{\text{eff}}\,t_s}\left[\frac{1}{2}\frac{\partial\varphi}{\partial z}(1+c_s^2) + \frac{1}{8}\frac{\partial c_s}{\partial z}(3c_s^2-1) - \frac{3}{4}\frac{c_s}{t_s}(c_s^2+1)\right], \tag{11}$$

where we have used the expression for N_c given in Eq. (5).

The final step is to employ the Euler–Lagrange equation,

$$\frac{d}{dz}\left(\frac{\partial L_g}{\partial q_z}\right) - \frac{\partial L_g}{\partial q} + \frac{\partial R_g}{\partial q_z} = 0, \tag{12}$$

where $q = A_s, T_s, \varphi_s$ or c_s, and the suffix z indicates the corresponding derivatives. For each q, we obtain an ordinary differential equation, resulting in a set of the following four coupled equations:

$$\frac{\partial A_s}{\partial z} = A_s\left[\frac{g_R}{2a_{\text{eff}}}P_p\left(1 - \frac{T_2^2}{T_s^2}\right) + \beta_{2s}\frac{c_s}{2T_s^2} - \frac{\alpha_s}{2} - \frac{\beta_{\text{TPA}}}{a_{\text{eff}}}P_p - \frac{\sigma_s}{2}\frac{\beta_{\text{TPA}}\tau_c P_p^2}{2h\nu_p a_{\text{eff}}^2}\right] - \frac{5\beta_{\text{TPA}}}{8\sqrt{2}}A_s^3, \tag{13}$$

$$\frac{\partial T_s}{\partial z} = -\beta_{2s}\frac{c_s}{T_s} + \frac{\beta_{\text{TPA}}}{4\sqrt{2}}A_s^2 T_s + \frac{g_R}{2a_{\text{eff}}}P_p\frac{T_2^2}{T_s}(1-c_s^2), \tag{14}$$

Table 1. Values of the Parameters Used for Numerical Calculations

Parameter Name	Symbol	Value
Waveguide length	L	1 cm
Waveguide linear loss	α_s	1 dB/cm
TPA parameter (nonlinear loss)	β_{TPA}	5×10^{-12} m/W
Nonlinear coefficient	n_2	6×10^{-18} m^2/W
Raman gain coefficient	g_R	7.6×10^{-10} m/W
Effective mode area	a_{eff}	0.4 μm^2
Carrier lifetime	τ_c	10 ns
FCA coefficient	σ_s, σ_p	1.45×10^{-21} m^2
Group-velocity dispersion	β_{2s}	20 ps^2/m
Free-carrier dispersion	μ	7.5
Signal wavelength	λ_s	1.55 μm
Signal pulse width	T_s	10 ps
Gain dispersion parameter	T_2	3 ps
Input peak power of signal	$P_s(0)$	1 mW
Input power of CW pump	$P_p(0)$	1 W
Input chirp	$C_s(0)$	0

$$\frac{\partial c_s}{\partial z} = -\frac{\beta_{2s}}{T_s^2}(1+c_s^2) - \frac{k_s n_2 A_s^2}{\sqrt{2}} + \frac{1}{2\sqrt{2}}\beta_{\mathrm{TPA}} A_s^2 c_s - \frac{g_R}{a_{\mathrm{eff}}} P_p \frac{T_2^2}{T_s^2}(1+c_s^2)c_s, \tag{15}$$

$$\frac{\partial \varphi_s}{\partial z} = \frac{\beta_{2s}}{2T_s^2} + \frac{5k_s n_2}{4\sqrt{2}} A_s^2 + \frac{2k_s n_2 P_p}{a_{\mathrm{eff}}} - \frac{\sigma_s \mu}{2}\left[\frac{\beta_{\mathrm{TPA}}\tau_c P_p^2}{2h\nu_p a_{\mathrm{eff}}^2}\right] + \frac{g_R P_p}{2a_{\mathrm{eff}}}\frac{T_2^2}{T_s^2} c_s. \tag{16}$$

Here, P_p varies with z and is obtained from Eq. (3). Equations (13)–(16) show explicitly that all pulse parameters may change during Raman amplification. Since phase changes are often not of practical interest, we ignore the phase equation in what follows. The pulse amplitude is of primary interest in practice as it governs the extent of Raman amplification. However, as is apparent from Eqs. (14) and (15), changes in the pulse amplitude invariably affect both the pulse width and the frequency chirp. As a result, the width and chirp of the signal pulse also change when its peak power changes through SRS, FCA, TPA or gain dispersion.

An advantage of our approach is that it is easy to see what nonlinear process affects a specific pulse parameter. For example, Eq. (14) shows that the Raman gain and FCA do not affect the pulse width, whereas TPA always leads to pulse broadening. The presence of the gain-dispersion parameter T_2 in Eqs. (13)–(16) shows explicitly that gain dispersion plays a significant role when pulse width is comparable to T_2. Since $T_2 = 3$ ps for silicon, the gain-dispersion effects become negligible for $T_s > 30$ ps but are significant for 10-ps pulses. In the following sections we study extensively the influence of different pulse parameters such as pulse width and frequency chirp on the process of Raman amplification

4. ROLE OF CARRIER LIFETIME

If one is interested only in the signal power, $P_s = |E_s|^2 a_{\mathrm{eff}}$, the following two coupled equations can be used to describe the Raman amplification process in a SOI waveguide [34]:

$$\frac{dP_p}{dz} = -\alpha_p P_p - \frac{\beta_{\mathrm{TPA}}}{a_{\mathrm{eff}}} P_p^2 - \left(\frac{\sigma_p \beta_{\mathrm{TPA}}\tau_c}{2h\nu_p a_{\mathrm{eff}}^2}\right) P_p^3, \tag{17}$$

$$\frac{\partial P_s}{\partial z} = P_s\left[\frac{g_R}{a_{\mathrm{eff}}} P_p\left(1 - \frac{T_2^2}{T_s^2}\right) + \frac{\beta_{2s} c_s}{T_s^2} - \alpha_s - \frac{2\beta_{\mathrm{TPA}}}{a_{\mathrm{eff}}} P_p - \frac{\sigma_s \beta_{\mathrm{TPA}}\tau_c P_p^2}{2h\nu_p a_{\mathrm{eff}}^2}\right] - \frac{5}{4\sqrt{2}}\frac{\beta_{\mathrm{TPA}} P_s^2}{a_{\mathrm{eff}}}. \tag{18}$$

Expression (18) shows how the peak signal power evolves

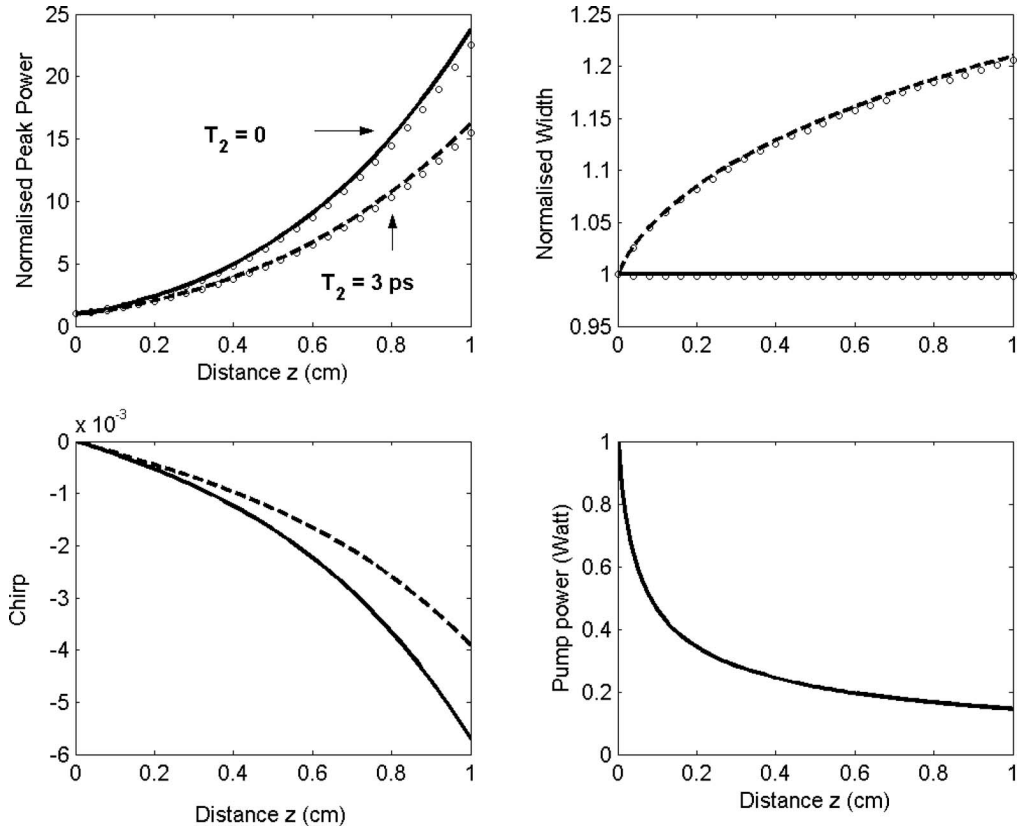

Fig. 1. Evolution of the peak power, pulse width, and chirp as a 10 ps wide signal pulse is amplified through SRS inside a silicon waveguide with parameters listed in Table 1. The gain dispersion effect is neglected for solid curves and is considered for dotted curves ($T_2 = 3$ ps). The pump power decreases in the same fashion in both cases. The open circles represent the numerical data based on the SSF algorithm.

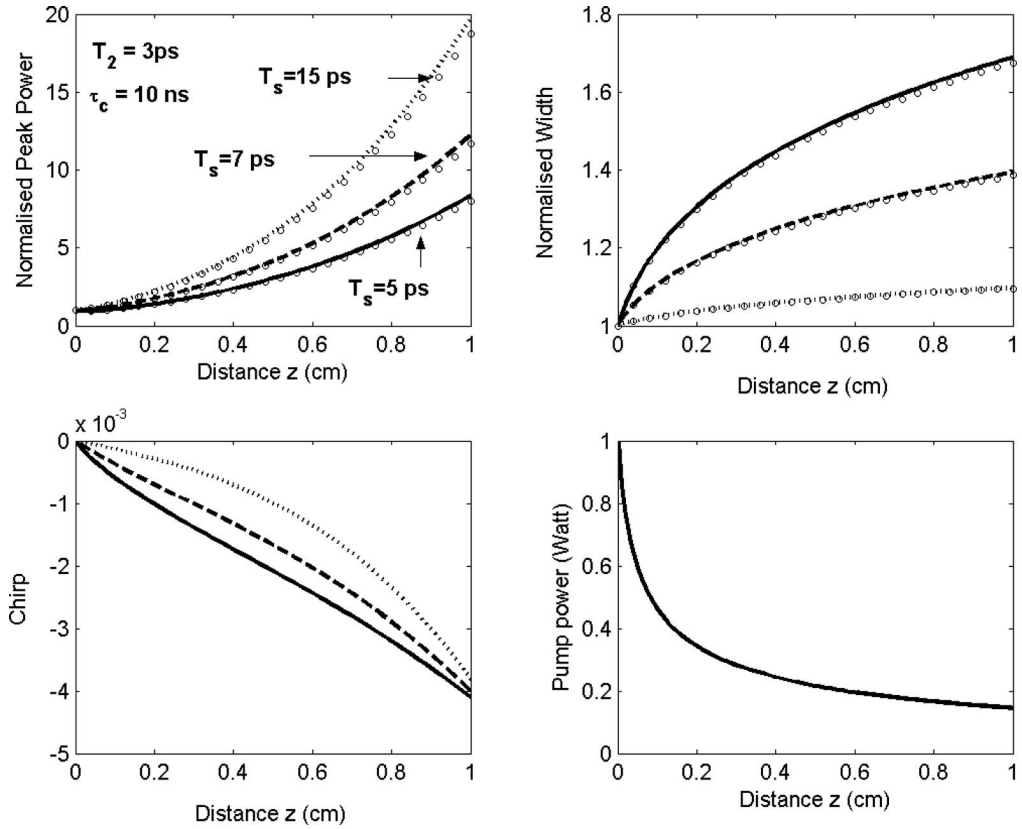

Fig. 2. Effect of different input pulse width on pulse parameters is represented. Open circles represent the corresponding numerical data based on the SSF algorithm. Parameters used are listed in Table 1.

inside a SOI waveguide. This equation differs from that obtained in earlier studies because it contains a new term $\beta_{2s}c_s/T_s^2$ that depends on the chirp parameter. It will reduce to the earlier result only if the input pulse is unchirped initially and remains so during amplification. This is generally not the case because the dispersion, SPM, and XPM chirp the pulse even if it is unchirped initially.

Notice that there are three distinct sources of TPA-induced losses in Eq. (18). The last term in Eq. (18) represents the TPA-induced nonlinear loss of the signal power and is often negligible for relatively weak signals. The other two TPA-related terms containing β_{TPA} depend on the pump power. The first one results from TPA occurring when one pump photon and one signal photon are absorbed simultaneously. The second one represents FCA induced by TPA-generated electron-hole pairs. This term is proportional to the square of the pump power. Thus, even though an increase in the pump power increases the Raman gain, it does not necessarily result in a net gain for the signal. Whether a net gain is possible depends on the carrier lifetime. This can be seen from Eq. (18), if we ignore the last term, assuming that the TPA of the signal is relatively small. Then, net gain is possible only if $\partial P_s/\partial z > 0$, or

$$\left(\frac{c_s\beta_{2s}}{T_s^2} - \alpha_s\right) + \left[g_R\left(1 - \frac{T_2^2}{T_s^2}\right) - 2\beta_{\mathrm{TPA}}\right]\frac{P_p}{a_{\mathrm{eff}}} - \frac{\sigma_s\beta_{\mathrm{TPA}}\tau_c P_p^2}{2h\nu_p a_{\mathrm{eff}}^2} > 0. \tag{19}$$

Solving this quadratic equation in pump power, we find that, if $\alpha_s > \beta_{2s}c_s/T_s^2$, the carrier lifetime should satisfy the condition

$$\tau_c < \frac{\left[g_R\left(1 - \frac{T_2^2}{T_s^2}\right) - 2\beta_{\mathrm{TPA}}\right]^2 h\nu_p}{2\sigma_s\beta_{\mathrm{TPA}}(\alpha_s - \beta_{2s}c_s/T_s^2)} \equiv \tau_{th}. \tag{20}$$

No such condition applies when $\alpha_s < \beta_{2s}c_s/T_s^2$. Equation (20) shows that the carrier lifetime should be less than a

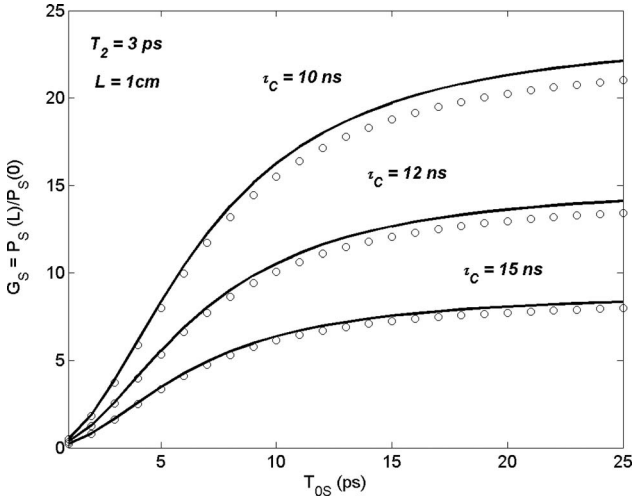

Fig. 3. Amplification factor, $G_s = P_s(L)/P_s(0)$, plotted as a function of the input pulse width for three different values of τ_c. Open circles represent the corresponding numerical data based on the SSF algorithm.

threshold value before CW pumping can be used for Raman amplification of the signal. A similar condition has been obtained in earlier studies [20]. The new and somewhat surprising result of our study is that the condition (20) depends on the both the chirp and dispersion parameters. In particular, if $\beta_{2s}c_s>0$, one can make τ_{th} relatively large. Moreover, the restriction on τ_c disappears altogether if $\alpha_s<\beta_{2s}c_s/T_s^2$. The physical reason why chirping can help the Raman amplification is that a pulse can compress inside a dispersive medium if the signs of the chirp and dispersion parameters are such that $\beta_{2s}c_s>0$. Equation (20) also indicates that gain dispersion reduces the threshold value. Note also that the value of τ_{th} changes along the waveguide length according to the dynamic evolution of pulse width and chirp.

5. NUMERICAL RESULTS

To illustrate the importance of our analysis, we focus on a concrete numerical example based on a SOI waveguide with the parameter values listed in Table 1. More specifically, a 10 ps wide signal pulse is amplified through SRS by pumping a 1 cm long silicon waveguide with 1 W of CW pump radiation. Figure 1 shows the evolution of the peak power, the width, with the condition of Raman amplification. The pulse is assumed to propagate in the normal-dispersion region of the SOI waveguide ($\beta_{2s}>0$) because this is often the case in practice, unless waveguide dimensions are reduced enough to shift the zero-dispersion wavelength below 1550 nm [27]. The solid curves show the case when the gain dispersion is ignored by setting $T_2=0$, while the dashed curves include gain dispersion using $T_2=3$ ps. In both cases, the pulse peak power increases because of the Raman gain provided by the pump, but the amount of amplification is significantly reduced for $T_2=3$ ps because the spectrum of 10 ps pulses is wide-enough that Raman gain is reduced in the spectral wings. The resulting spectral narrowing also increases the pulse width as is shown clearly in Fig. 1.

The preceding results show that a variational approach allows one to obtain considerable physical insight in designing Raman amplifiers based on SOI waveguides. However, one may ask how trustworthy this approach is, because it assumes that a signal pulse maintains a Gaussian shape during its amplification. To answer this question, we have solved Eq. (1) numerically with the well-known split-step Fourier (SSF) method [35] and compared our approximate semi-analytic results with the results (shown by circles) obtained with full numerical simulations. From now on, most of our analytical results will be verified by the numerical data based on the SSF algorithm.

The initial pulse width plays an important role as indicated in Fig. 2, where changes in the pulse width, chirp, and peak power along the waveguide length are shown for three values of input pulse widths. The net amplification is gradually reduced for shorter pulses. Since the spectral bandwidth becomes wider for shorter pulses, the gain dispersion dominates more and more for shorter pulses and result in less amplification. To visualize the effect of pulse width more clearly, we show in Fig. 3 the Raman amplification for three different carrier lifetimes. In all cases, the gain is reduced sharply for shorter pulses. Note also that the peak gain saturates for pulses wider than 20 ps. This is expected because the spectral bandwidth of such pulses becomes narrow enough that all spectral components experience nearly the same gain. The numerical results (open circles) agree reasonably well with the analytical results (solid curves). The minor discrepancy between the two is related to the assumption inherent in the variational method that the pulse does not change its shape during its propagation along the waveguide.

Figure 4 shows the evolution of the peak power of a 10 ps signal pulse along the waveguide length. The results are computed using the semi-analytical (solid curves) and numerical (open circles) methods for three different carrier lifetimes. Except for minor differences, the variational approach reproduces most of the features obtained with the much more time-consuming SSF method. As can be seen in Fig. 4, the numerical value of the carrier lifetime τ_c affects the Raman amplification process considerably. This behavior is related to the detrimental effects of the buildup of the free-carrier population within the SOI waveguide. As seen in Eq. (5), the car-

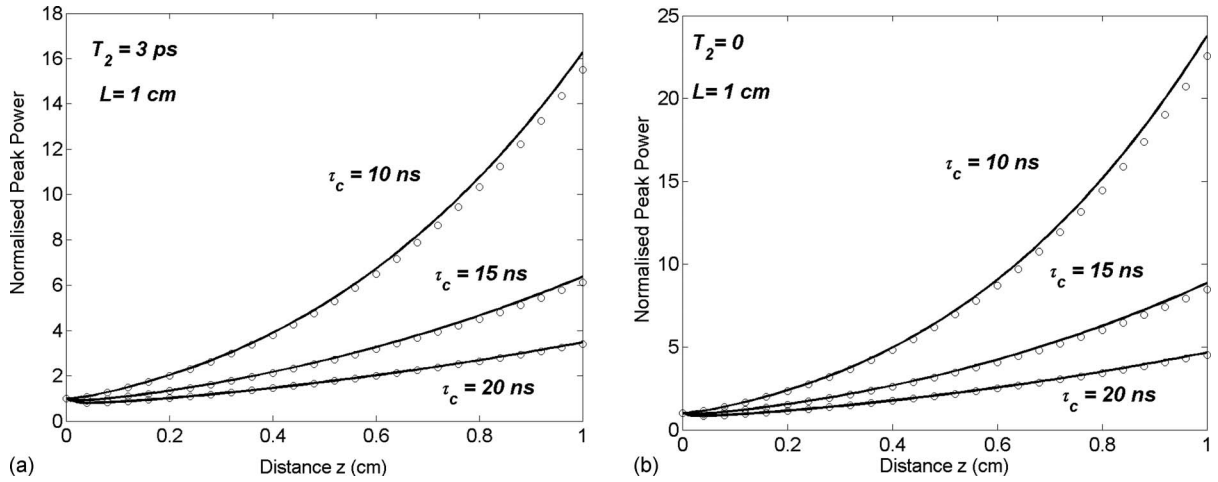

Fig. 4. Evolution of the peak signal power along the waveguide during amplification, for three different values of the carrier lifetime. In (a) gain dispersion is considered where as in (b) it is absent. Open circles represent the corresponding values obtained numerically with the SSF algorithm.

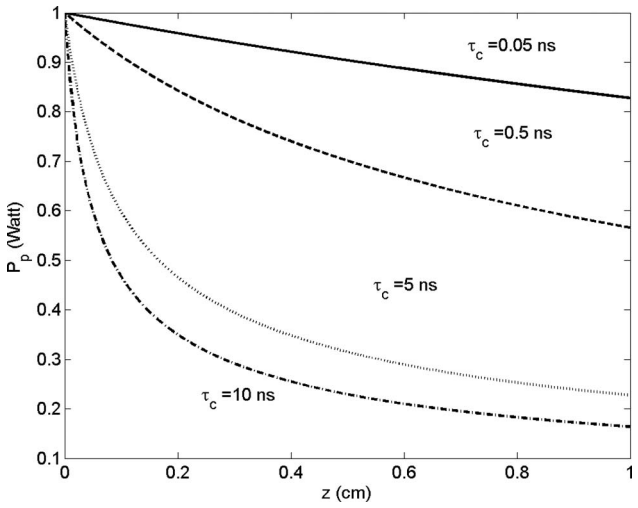

Fig. 5. Evolution of pump power along the waveguide length for different values of τ_c ranging from 50 ps to 10 ns.

rier density N_c is directly proportional to τ_c. For a shorter value of the carrier lifetime, N_c is smaller. As a result, losses of the pump induced by FCA also decrease. Figure 5 shows how the pump power decreases along the waveguide length for several values of τ_c ranging from 0.05 to 10 ns. Since more pump power is available, especially near the output end of the waveguide, the signal is amplified considerably more for shorter values of τ_c.

We now focus on the peak power $P_s(L)$ of the amplified signal pulses at the waveguide output. In order to take into account the pulse dynamics fully, we solve the set of Eqs. (13)–(18) simultaneously using Matlab software with parameter values given in Table 1. Figure 6 shows the net amplification factor, defined as $G_s=P_s(L)/P_s(0)$, as a function of the input pump power in the cases of infinite (solid curves) and finite (dashed curves) gain bandwidth with an input peak power of 1 mW for three different carrier lifetimes. In all cases, an increase in the pump power does not always enhance the signal gain; rather, after a certain

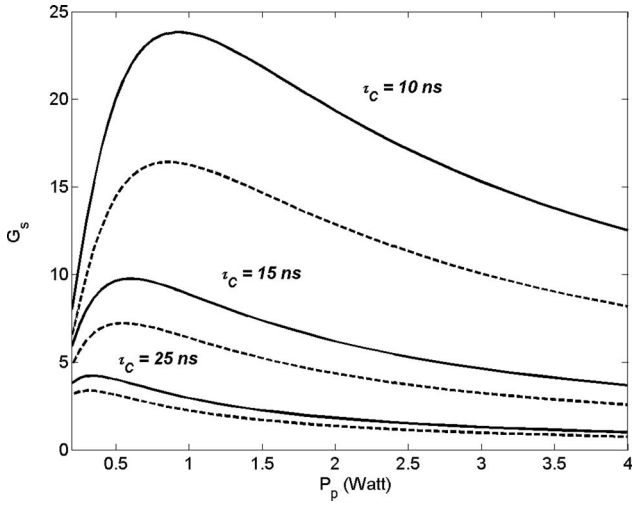

Fig. 6. The amplification factor, $G_s=P_s(L)/P_s(0)$, plotted as a function of the pump power for three different values of τ_c. Solid curves represent the amount of gain considering infinite gain band width whereas dashed curves signify the same for finite bandwidth.

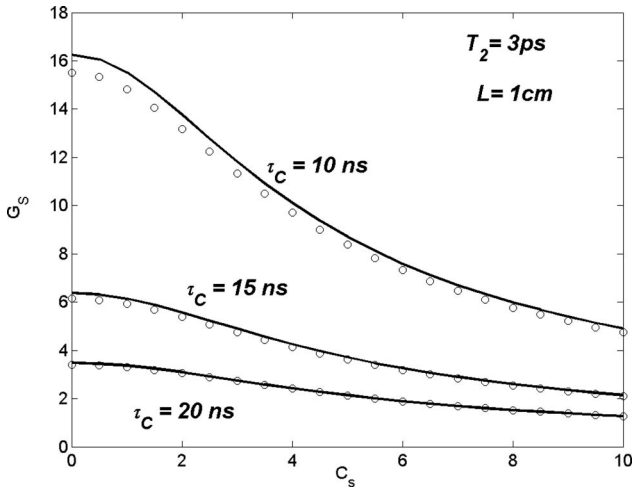

Fig. 7. The amplification factor, $G_s=P_s(L)/P_s(0)$, plotted as a function of input chirp for three different values of τ_c. Open circles represent the corresponding values obtained numerically with the SSF algorithm.

value of the input pump power, the effective signal gain starts to decrease. This feature can be attributed to an increase in TPA, and the resulting FCA, with increasing pump powers. The important point to note is that the amplification factor is always reduced because of a relatively narrow Raman-gain bandwidth. For example, the maximum value of G_s is reduced from 24 to 16 when the carrier lifetime is 10 ns.

Next we evaluate the effect of chirp on pulse amplification. Figure 7 shows that the amplification factor is gradually reduced for chirped pulses. With increasing linear chirp, the spectral bandwidth of pulses increases so much that only a small central portion of the pulse spectrum falls within the Raman gain bandwidth and is amplified by the Raman effect. The amplification factor is gradually reduced because of that. In Fig. 8, we show an interesting phenomenon indicating the compression of pulses with increasing chirp. For a finite gain bandwidth, the width reduction occurs because the pulse is linearly chirped, and the central part is amplified most as also evi-

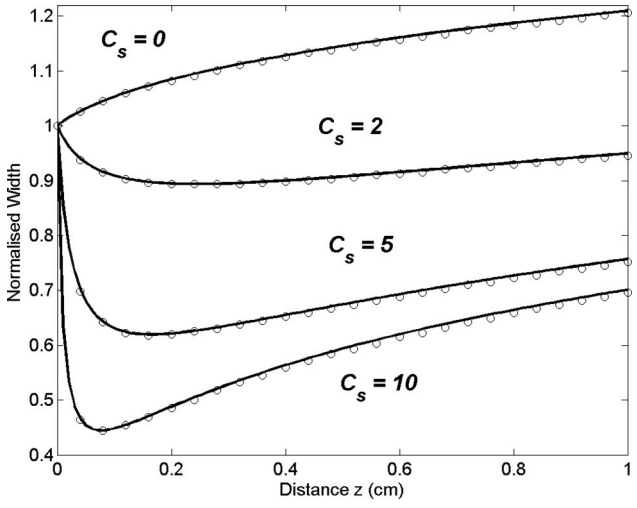

Fig. 8. Evolution of normalized pulse width for different initial chirping. Open circles represent the corresponding values obtained numerically with the SSF algorithm.

dent from the numerical results (shown by circles). In contrast, for initially unchirped pulses, the width increases due to the influence of gain dispersion effect. Thus, one important conclusion is that a suitable amount of chirp can maintain the pulse shape at the cost of gain.

6. CONCLUSIONS

In this work we have studied the Raman amplification of picoseconds optical pulses under CW pumping of a SOI waveguide. The effects of a finite Raman-gain bandwidth are included in the present discussion together with the effects of TPA and FCA. The amplification problem is solved analytically using a variational technique that makes use of the RDF for handling the Raman gain and various sources of optical losses. The use of RDF allowed us to include the effects of TPA, FCA, linear loss, and gain dispersion on the process of Raman amplification. Our analysis shows that a finite bandwidth of the Raman-gain spectrum significantly reduces the amount of amplification and leads to pulse broadening. The new feature compared to most other previous studies is that we allow for changes in the pulse width and the frequency chirp during Raman amplification. Our work shows that a suitable input chirp can effectively reduce this pulse broadening.

ACKNOWLEDGMENTS

The authors thank H. S. Maiti of CGCRI for his continuous encouragement, guidance, and support during this work. We also thank the staff members of the Fiber Optic Laboratory at CGCRI for their unstinted cooperation and help. S. R. is indebted to the Council of Scientific and Industrial Research (CSIR) for financial support in carrying out this work. The work of G.P.A. is supported by the National Science Foundation (NSF) award ECCS-0801772.

REFERENCES

1. B. Jalali and S. Fathpour, "Silicon photonics," J. Lightwave Technol. **24**, 4600–4615 (2006).
2. H. K. Tsang, C. S. Wong, and T. K. Liang, "Optical dispersion, two-photon absorption and self-phase modulation in silicon waveguides at 1.5 μm wavelength," Appl. Phys. Lett. **80**, 416–418 (2002).
3. Ö. Boyraz, P. Koonath, V. Ranghanathan, and B. Jalali, "All optical switching and continuous generation in silicon waveguides," Opt. Express **12**, 4094–4102 (2004).
4. R. Claps, D. Dimitropoulos, V. Raghunathan, Y. Han, and B. Jalali, "Observation of stimulated Raman amplification in silicon waveguide," Opt. Express **11**, 1731–1739 (2003).
5. T. K. Liang and H. K. Tsang, "Role of free carriers from two-photon absorption in Raman amplification in silicon-on-insulator waveguides," Appl. Phys. Lett. **84**, 2745–2747 (2004).
6. R. Claps, V. Raghunathan, D. Dimitropoulos, and B. Jalali, "Influence of nonlinear absorption on Raman amplification in silicon waveguides," Opt. Express **12**, 2774–2780 (2004).
7. A. Liu, H. Rong, M. Paniccia, O. Cohen, and D. Hak, "Net optical gain in low loss silicon-on-insulator waveguide by stimulated Raman scattering," Opt. Express **12**, 4261–4267 (2004).
8. T. K. Liang and H. K. Tsang, "Nonlinear absorption and Raman scattering in silicon-on-insulator optical waveguides," IEEE J. Sel. Top. Quantum Electron. **10**, 1149–1153 (2004).
9. H. Rong, A. Liu, R. Nicolaescu, M. Paniccia, O. Cohen, and D. Hak, "Raman gain and nonlinear optical absorption measurement in a low-loss silicon waveguide," Appl. Phys. Lett. **85**, 2196–2198 (2004).
10. T. K. Liang and H. K. Tsang, "Efficient Raman amplification in silicon-on-insulator waveguides," Appl. Phys. Lett. **85**, 3343–3345 (2004).
11. M. Krause, H. Renner, and E. Brinkmeyer, "Analysis of Raman lasing characteristics in silicon-on-insulator waveguides," Opt. Express **12**, 5703–5710 (2004).
12. Q. Xu, V. R. Almeida, and M. Lipson, "Demonstration of high Raman gain in submicrometer-size silicon-on-insulator waveguide," Opt. Lett. **30**, 35–37 (2005).
13. R. Jones, H. Rong, A. Liu, A. W. Fang, M. J. Paniccia, D. Hak, and O. Cohen, "Net continuous wave optical gain in a low loss silicon-on-insulator waveguide by stimulated Raman scattering," Opt. Express **15**, 519–525 (2005).
14. H. Rong, A. Liu, R. Jones, O. Cohen, D. Hak, R. Nicolaescu, A. W. Fang, and M. J. Paniccia, "An all-silicon Raman laser," Nature **433**, 292–294 (2005).
15. H. Rong, R. Jones, A. Liu, O. Cohen, D. Hak, A. W. Fang, and M. J. Paniccia, "A continuous-wave Raman silicon laser," Nature **433**, 725–728 (2005).
16. A. Liu, H. Rong, R. Jones, O. Cohen, D. Hak, and M. J. Paniccia, "Optical amplification and lasing by stimulated Raman scattering in silicon waveguide," J. Lightwave Technol. **24**, 1440–1448 (2006).
17. H. Fukuda, K. Yamada, T. Shoji, M. Takahashi, T. Tsuchizawa, T. Watanabe, J. Takahashi, and S. Itabashi, "Four wave mixing in silicon wire waveguides," Opt. Express **13**, 4629–4637 (2005).
18. L. Yin, Q. Lin, and G. P. Agrawal, "Soliton fission and supercontinuum generation in silicon waveguides," Opt. Lett. **32**, 391–393 (2007).
19. L. Yin and G. P. Agrawal, "Impact of two-photon absorption on self-phase modulation in silicon waveguides," Opt. Lett. **32**, 2031–2033 (2007).
20. Q. Lin, O. J. Painter, and G. P. Agrawal, "Nonlinear optical phenomena in silicon waveguides: Modeling and applications," Opt. Express **15**, 16604–16644 (2007).
21. P. Spirito, S. Daliento, A. Sanseverino, L. Gialanella, M. Romano, B. Limata, R. Carta, and L. Bellemo, "Characterization of recombination center in Si epilayers after He implantation by direct measurement of local lifetime distribution with the AC lifetime profiling technique," IEEE. Elec. Dev. Lett. **25**, 602–604 (2004).
22. Y. Liu and H. K. Tsang, "Nonlinear absorption and Raman gain in helium-ion implanted silicon waveguides," Opt. Lett. **31**, 1714–1716 (2006).
23. V. Sih, S. Xu, Y. Kuo, H. Rong, M. Paniccia, O. Cohen, and O. Raday, "Raman amplification of 40 Gb/s data in low-loss silicon waveguides," Opt. Express **15**, 357–362 (2007).
24. H. Goldstein, *Classical Mechanics*, 2nd ed. (Narosa Publishing House, 2001).
25. S. Roy and S. K. Bhadra, "Solving soliton perturbation problems by introducing Rayleigh's dissipation function," J. Lightwave Technol. **26**, 2301–2322 (2008).
26. D. Dimitropoulos, R. Jhaveri, R. Claps, J. C. S. Woo, and B. Jalali, "Lifetime of photogenerated carriers in silicon-on-insulator rib waveguides," Appl. Phys. Lett. **86**, 071115 (2005).
27. L. Yin, Q. Lin, and G. P. Agrawal, "Dispersion tailoring and soliton propagation in silicon waveguides," Opt. Lett. **31**, 1295–1297 (2006).
28. X. Chen, N. C. Panoiu, and M. Osgood, "Theory of Raman-mediated pulsed amplification in silicon-wire waveguide," Int. J. Quantum Chem. **42**, 160–170 (2006).
29. L. Yin, J. Zhang, P. M. Fauchet, and G. P. Agrawal, "Ultrabroadband parametric generation and wavelength conversion in silicon waveguides," Opt. Express **14**, 4786–4799 (2006).
30. R. Dekker, A. Driessen, T. Wahlbrink, C. Moormann, J. Niehusmann, and M. Först, "Ultrafast Kerr—induced all-optical waveguide conversion in silicon waveguides using

1.55 μm femtosecond pulses," Opt. Express **14**, 8336–8346 (2006).
31. V. Passaro and F. D. Leonardis, "Space-time modeling of Raman pulses in silicon-on insulator optical waveguides," J. Lightwave Technol. **24**, 2920–2931 (2006).
32. E. Tien, N. S. Yuksek, F. Qian, and O. Boyraz, "Pulse compression and modelocking by using TPA in silicon waveguides," Opt. Express **15**, 6500–6506 (2007).
33. D. Anderson, "Variational approach to nonlinear pulse propagation in optical fibers," Phys. Rev. A **27**, 3135–3145 (1983).
34. H. Rong, S. Xu, Y. H. Kuo, V. Sih, O. Cohen, O. Raday, and M. Paniccia, "Low-threshold continuous-wave Raman silicon laser," Nature Photonics **1**, 232–237 (2007).
35. G. P. Agrawal, *Nonlinear Fiber Optics*, 4th ed. (Academic, 2007).